

Oxidation Lifetimes: Experimental Results and Modeling

I. G. Wright, B. A. Pint, L. M. Hall*, and P. F. Tortorelli
Oak Ridge National Laboratory
Oak Ridge, TN 37831

Abstract

Experimental results for high-temperature alloys with excellent oxidation resistance strongly suggest that their oxidation behavior involves several distinct stages that are not well addressed in current models. An approach is suggested that relies on breaking the 'steady-state' oxidation stage into multiple stages. In higher-temperature experiments, two such stages are clearly observed, whereas at more relevant, lower temperatures, these stages are more difficult to observe within reasonable experimental times. Because this approach attempts to more closely model the observed oxidation behavior, it requires input on the rate of oxidation and the rate law exponent for each stage, as well as a criterion for changing from one stage to the next. Thus, it is necessary to improve the mechanism-based description of the oxidation behavior in each stage. Initial results show reasonable predictions using this methodology for one alloy (MA956HT). However, extensive work will be required to determine the real potential for this approach, particularly for lower temperatures. While it is recognized that other complicating phenomena have been observed, such as effects of specimen thickness and cycle frequency on oxidation lifetime, these have not been incorporated into this modeling effort.

Introduction

Failure of a component exposed to a high-temperature corrosive environment will occur if the corrosion rate is sufficient to reduce the thickness of the load-bearing section below that needed to sustain the imposed mechanical load. The main aim of any model of oxidation behavior should be to predict the maximum rate of section thinning as a function of alloy properties, temperature, time, and mode of attack. However, the monotonic rate of loss of section thickness from high-temperature oxidation is not usually the life-determining factor in applications where the alloys function as intended. Under such conditions, rapid metal loss and section thinning will occur only when the alloy surface becomes depleted in the protective oxide-forming elements below the minimum requirement by, for instance, consumption by the scale-forming process. This process is known as breakaway oxidation and can lead to rapid component failure. How available understanding of alloy oxidation behavior is translated into reliable information for practical use is the concern addressed in this paper.

*Rochester Institute of Technology, NY.

There exists an urgent need for oxidation lifetime modeling to provide guidance for the quantification of the high-temperature oxidation behavior of alloys in a form that is useful for the practical application of the alloys, and to remedy the poor state of technology transfer in this area among scientists, designers, and engineers. At the very least, a model for the high-temperature oxidation behavior of an alloy should be capable of predicting its useful service life as a function of alloy type, component thickness, and temperature. Extension to include the effects of temperature fluctuation and changes in oxidizing environment also would be desirable.

Values of oxidation lifetimes serve the purpose of quantifying the overall high-temperature environmental resistance of alloys that form protective oxide scales. Using defined criteria for end of life, oxidation lifetimes can be measured but, for certain alloys and service conditions, these times can be extraordinarily long. Therefore, the ability to accurately and robustly model lifetimes is needed so as to (1) qualify materials for service at high temperatures based on a limited set of measurements and knowledge of the starting materials (composition, dimensions), and (2) serve as a means to guide alloy selection and component design for extended high-temperature service.

Systematic modeling of high-temperature oxidation behavior is obviously needed for lifetime prediction. However, even for simple alloys, this type of modeling is hindered by the need to describe a relatively complex sequence of processes in terms that can be readily quantified, yet, which relate to the observed behavior under various conditions. Several approaches for modeling oxidation lifetime beyond the use of simple rate laws have been put forward¹⁻⁵ and have successfully described performance in certain cases. However, no one approach to lifetime modeling seems *a priori* to be wholly appropriate; a modest-to-moderate amount of experimentation for a particular material system is needed to provide the input parameters for predictions of oxidation lifetime. The goal of a single robust model for predicting oxidation lifetime that incorporates all of the most important factors and is applicable to a wide range of materials and conditions has not yet been achieved. In this paper, some of these factors are reviewed and related to long-term oxidation data for an alumina-forming alloy, Special Metals (Huntington, West Virginia, USA) Alloy MA956HT, in air at 1000-1300°C, in terms of kinetics and time-to-breakaway. Following Quadackers, Bennett, et al.³⁻⁵ emphasis is on Al reservoir and power law consumption by oxidation. The data sets involve total mass gain (specimen mass gain plus mass of any spalled oxide) instead of specimen mass gain alone, and time to breakaway oxidation versus specimen thickness.

Important Factors for an Oxidation Model and Related Experimental Results

Calculating the Alloy Service Lifetime

Modeling of the oxidation-governed lifetime of a high-temperature alloy requires the definition of two main parameters: (i) a criterion that signals the end of useful life, and (ii) a readily measured or calculated parameter that tracks the input data used by the criterion.

End of Life Criterion: As indicated earlier, the end of life criterion for many components is the point where sufficient cross-section has been lost that they can no longer sustain the required mechanical load. This may be particularly true for conditions that give rise to rapid oxidation for components with thin-cross sections, or where internal attack occurs and reduces the strength of the component. Typically, the alloys used for high-temperature service are designed to form protective Cr_2O_3 or Al_2O_3 scales by the addition of Cr or Al, or combinations of these and other elements. However, when the needs for high-temperature strength and corrosion resistance are combined, the content of protective scale-forming elements is often close to the minimum requirement in order to maximize alloy strength. In such cases, a moderate amount of oxidation can sufficiently deplete the alloy in Cr or Al so that breakaway oxidation can ensue, resulting in rapid metal consumption. In this case, a typical criterion for breakaway oxidation for a simple binary alloy AB designed to form a protective oxide $\text{B}_2\text{O}_{z\text{B}}$ (where valence of B is Z) is the point when the activity/concentration of B at the alloy-oxide interface (C_{Bi}) falls below the kinetically-determined minimum required to maintain the protective oxide (C_{Bi^*}).

Tracking Parameter: For the two alternative end of life criteria described above, the tracking parameters would be very different. For the critical cross-section criterion, the specimen thickness would be the tracking parameter; this is the parameter of concern in, for instance, the ASSET model². Specimen thickness change could possibly be inferred from mass change data but, particularly for the case of internal oxidation, microstructural information would be required. For the case of depleting B to a critical level, the key parameter would be the rate of consumption of B. This value could be calculated from mass change data or, if the relevant oxidation behavior parameters for the alloy were known, could be calculated solely from a knowledge of the temperature history. However, for the most oxidation-resistant alloys of nominal cross-section (1-5 mm), measuring the thickness change will yield little information until the alloy goes into breakaway oxidation (which would signal end of service life). For example, Fig. 1 shows a cross-section of the scale formed on MA956HT after 10,000h at 1100°C in air (see, also, ref. 6). No internal oxidation was observed and very little thickness change could be

measured. However, the mass change data could be used to calculate the amount of B (Al) consumed after this exposure, since the scale formed was predominantly Al_2O_3 at this stage. Because the current focus is on modeling the performance of the most oxidation-resistant alloys, the following discussion will deal mainly with predicting the consumption rate of B until the breakaway condition (i.e., $C_{B_i} = C_{B_i^*}$) is reached.

Calculating the Available Reservoir of B

One essential parameter required for this approach is the absolute reservoir of B available. Ideally, the amount of B available to take part in the oxidation process is given by the density and thickness of the component and the difference between the initial and final B contents ($C_{B_0} - C_{B_i^*}$). However, this assumes that the rate of transport of B in the alloy is faster than its rate of consumption at the alloy-oxide interface. This condition may be true for Al in most alumina-forming alloys at high temperatures (e.g. refs. 3-5), especially during steady-state oxidation. However, in many alloys (particularly chromia-formers) at temperatures typically encountered in service, this condition may not be fulfilled. This represents a critical issue for modeling the performance of chromia-forming alloys, and is beyond the current scope of work and of this paper. Instead, the focus here is on the issues involved in describing and modeling the consumption of Al in alumina-forming alloys at high temperatures.

Calculating the Rate of Consumption of B

The consumption of B (W_B/A , mass per unit area) by an idealized oxidation process can be described by:

$$W_B/A = kt^n \quad (1)$$

where k is the rate constant for the oxidation process, t is the time that the oxidation process is operating, and n is the rate law exponent. However, the process suggested by eqtn. 1 does not fully account for the oxidation behavior exhibited by many practical alloys, which may be represented as a series of events: (1) a transient oxidation stage, (2) a period of steady state oxidation, (3) a period of modified steady-state oxidation, often observed during thermal-cycling where a process such as oxide spallation-regrowth occurs with faster oxidation rates than the normal steady-state period, and finally (4) breakaway oxidation. Pieraggi has pointed out the need to isolate transient effects from the steady-state rate constant.⁷ The modified steady-state period (Stage 3) is described in the COSP model¹ as a near-linear mass loss, but in other alloy systems may result in mass gains or other, more complex behavior.⁸

Regardless of exactly what happens during Stage 3, this behavior is most likely observed for many high-temperature alloys. Although it is poorly understood, it plays a critical role in lifetime predictions.

There are numerous experimental results supporting the importance of a second steady-state stage. For example, as shown in refs. 3 and 4, solving a simplified equation of supply of B versus consumption rate as described solely by eqn. 1 leads to the conclusion that the time to breakaway should be proportional to the component thickness to the power (n) which, for parabolic behavior ($n=0.5$) would be 2. However, as illustrated in Figs. 2-4 for several alumina-formers, the n values obtained experimentally are far from this value, ranging from 0.39 to 1.37. These lifetime data were obtained under cyclic oxidation conditions: MA956HT, Kanthal APM, and Fe-28Al-2Cr+Hf during 100 h cycles at 1300°C, and for Haynes 214 and ORNL-fabricated FeCrAl+ La₂O₃ and FeCrAl+Y₂O₃ during 1h cycles at 1200°C (see Table I for compositions). Any cracking or spallation of scale resulting from the cyclic nature of these tests might be expected to modify the assumptions implicit in parabolic oxidation behavior. For the alloys studied, since no scale spallation was observed during Stage 2, the simplifying assumption was made that any modification of diffusion transport in the scales resulting from cracking was short-lived, so that any perturbation from parabolic behavior was negligible. This assumption will have to be revisited for alloys that exhibit more obvious effects from thermal cycling during Stage 2. The experimental data discussed here were obtained using a technique of exposing samples in individual alumina crucibles in a cyclic test which yielded information on the total metal consumption, so that experimental problems with measuring the amount of spallation were avoided.⁸ The reason for the use of such high temperatures was to generate failure in a reasonable time; testing at lower temperatures would require at least an order of magnitude increase in the test times.

Complicating Factors

While in most cases the overall oxidation processes of like alloys are assumed to be similar, variables such as the physical dimensions of the specimen, initial surface finish, microstructure of the alloy/strengthening phases present, and the temperature dependence of the mechanical properties of the alloy substrate can significantly modify the duration of the different stages of oxidation, the morphology of the oxide formed, or the time to onset of oxide spallation. While not intended to be a comprehensive catalogue of such complicating factors, Table II lists some of the more common assumptions, and factors that can complicate or confound these assumptions.

A Multistage Model

Analysis of a data set of total and specimen mass gain for MA956HT oxidized in 100 h cycles in air at 1300°C clearly indicated that several mass-gain stages occurred during the oxidation lifetime, Fig. 5. As suggested in Fig. 6, if any initial period of transient oxidation is ignored, two major stages can be defined. An initial attempt to describe such multistage oxidation behavior involves replacing the single k and n value in eqtn. 1 by expressions to account for the consumption of B in each stage, such as:

$$W_B/A = k_1 t_1^{n_1} + k_2 t_2^{n_2} + k_3 t_3^{n_3} \quad (2)$$

where t_1 , t_2 , and t_3 are the times spent in each of the stages of oxidation: (1) transient, (2) steady state and (3) modified steady-state. Additional stages could be included if necessary (and justified mechanistically), but even this expression rapidly becomes difficult to manipulate. For any particular alloy and oxidation conditions, the time in each stage may be widely different. For the alloys considered here, the transient stage appears short-lived, thus Stages 2 and 3 represent the dominant contributions to service lifetime. Of these parameters, the value of $(k_2 t_2^{n_2})$ is the most easily obtained (for example, from the experimental data shown in Fig. 5), even at lower temperatures. Depending on the alloy and oxidation conditions, Stage 3 ($k_3 t_3^{n_3}$) may be experimentally observed or it may have to be predicted because it only initiates after extremely long exposures at lower temperatures, so that it is not feasible to conduct experiments of appropriate duration.

Modified Calculation for Oxidation-Governed Lifetime

The time spent in oxidation according to a simple parabolic rate law (Stage 2) is readily calculated from the parabolic rate constant:

$$t_2 = (S_{2-3} / k_2)^{1/n_2} \quad (3)$$

where:

ρ_A is the density of alumina = 3965 mgcm⁻³ (used in the absence of an actual value for a thermally-grown oxide),

x_{2-3} is the oxide thickness at the transition from Stage 2 to Stage 3 (μm), as determined from the experimental data (c.f. Fig. 5) when possible, and

S converts mass gain to mass of Al₂O₃ formed = 0.4707.

The time spent in the third stage of oxidation is assumed to be governed by the amount of available Al in the alloy. This requires a knowledge of the amount of Al consumed during the parabolic oxidation stage, which is obtained by equating the duration of the parabolic stage to the change in total Al content in the alloy, after Quadakkers et al.³⁻⁴:

$$t_2 = (10^{-4} S_{2-3} A/k_2)^{1/n_2} = [(C_{B_0} - C_{B_2})d / 200Mk_2]^{1/n_2} \quad (4)$$

where:

C_{B_0} = the initial Al content of the alloy = 5.9 wt %,

C_{B_2} = the Al content of the alloy at the end of the parabolic oxidation stage (wt %),

C_{B_b} = the Al level at which a protective Al_2O_3 can no longer form (and, for the class of alloys studied here, = $C_{B_i^*}$) (wt %),

d = the thickness of the section being oxidized (cm),

M = the density of the alloy = 7200 mg/cm³, and

M = converts mass gain to Al consumed = 1.1246.

Solving for C_{B_2} yields:
$$C_{B_2} = C_{B_0} - 0.02MS_{2-3} A/d \quad (5)$$

Hence, the oxidation lifetime (time to breakaway, t_b), assuming a section thickness sufficient to allow oxidation to proceed through Stage 3, is:

$$t_b = t_2 + t_3 = (10^{-4} S_{2-3} A/k_2)^{1/n_2} + [(C_{B_2} - C_{B_b})d / 200Mk_2]^{1/n_3} \quad (6)$$

$$= (10^{-4} S_{2-3} A/k_2)^{1/n_2} + \{[(C_{B_0} - C_{B_b})d / M - 0.02MS_{2-3} A] / (200Mk_3)\}^{1/n_3} \quad (7)$$

Additional stages could be added in a similar manner.

Applying a Multi-Stage Model

As a first step in testing the proposed approach and in examining the underlying assumptions to determine what modifications are needed to broaden its applicability, the multistage consumption model was applied to the MA956HT data set for cyclic oxidation at 1300°C, shown in Figs. 2 and 5, from which actual values of oxidation-limited lifetime as a function of specimen thickness were obtained (Table III).

Any transient oxidation stage was ignored, and the consumption was based on the two stages suggested in Fig. 6. Values of n_2 and n_3 were obtained by log-log slope analysis of the data for each of the seven specimens. The average values for the data set of n_2 and n_3 were 0.52 and 1.03, respectively (see Table IV), suggesting essentially parabolic and linear oxidation behavior. Further, Stage 2 terminated at an average mass gain equivalent to an oxide thickness (δ_{2-3} , assumed all Al_2O_3) of 29 μm . Values of k_2 and k_3 were obtained from parabolic and linear plots of the respective segments of each data set, and the average values determined (Table IV). These rate constants were input to eqn. 7, along with $n_2 = 0.5$, and $n_3 = 1.0$, and used to calculate the oxidation-limited lifetime as a function of specimen thickness. The result is shown in Fig. 7, and was found to significantly over-predict the specimen lifetimes.

Since a parabolic Stage 2 appeared entirely consistent with the experimental kinetic and morphological data, it was considered that the more likely source of the underestimation of the rate of Al consumption was the assumption of a strictly linear third stage. Examination was made of the sensitivity of eqn. 7 to changes in the value of n_3 (and the linked values of k_3), using values of k_3 calculated from plots of weight gain versus t^{1/n_3} . As shown in Table V, for all combinations of n_3 and k_3 for values of n_3 ranging from 1.00 to 1.10, eqn. 6 overestimated life by approximately 41 percent, indicating that the use a single process to describe Stage 3 resulted in a poor match to the experimental observations.

The sensitivity of the two-stage fit to the main variables was then re-examined by using the base values obtained from the experimental data (see Table IV), and allowing one of the variables n_3 , k_3 , δ_{2-3} , and C_{Bb} to vary, with the results shown in Fig. 8. This indicated that an excellent match to the experimentally-observed lifetimes could be obtained if n_3 was increased to 1.06, or if k_3 was increased by a factor of 1.5, or if the value of C_{Bb} was increased to 2.5 percent (see Table V). Note that the use of the experimentally-determined average value of k_3 (1.03) led to an over-prediction of lifetimes. Of these changes, the increases required in k_3 and C_{Bb} to obtain a fit to the experimental data were considered to be unrealistic, based on the range of consistency of the experimentally-observed values of k_3 among the seven specimens studied and the general acceptance that C_{Bb} for alloys of this type is less than 2.0 percent³⁻⁵. Since it is possible that Al consumption in Stage 3 is driven by more than one process occurring simultaneously (or sequentially), such as scale spallation at specimen ends and scale cracking and rehealing on the parallel sides, its description by a single, linear process probably is overly simplistic. A process involving localized loss of scale followed by reoxidation can lead to an essentially linear overall oxidation rate for the area of surface affected but, as discussed in the COSP model¹ and in models for erosion-augmented oxidation⁹, knowledge is needed of the area fraction over which this process occurs, the thickness of oxide lost in each event, and the frequency of the spallation events. At present, there is insufficient experimental evidence to provide such information. Hence, it was

considered that augmentation of the Stage 3 rate exponent (to suggest a more complex process than scale spallation alone) was a reasonable modification of the model until an acceptable mechanism-based description of Stage 3 is available. The rate exponent in Stage 3 then becomes $(n_3 + f_{n_3})$; in the case of MA956HT at 1300°C, $n_3 = 1.00$ and $f_{n_3} = 0.06$. The lifetimes calculated at 1300°C as a function of specimen thickness using the 2-stage model modified by an augmentation factor are shown in Table VI and Fig. 7.

The next step was to examine the ability of the modified 2-stage model to predict the performance of the same alloy at lower temperatures, using the experimental results shown in Fig. 9. At 1200°C, the experimental total mass change data appeared to fit similar trends as at 1300°C, although the form of the specimen mass change curve was different from that at 1300°C; since only one data set was available where a specimen had accumulated sufficient exposure time at 1200°C, this trend will be further examined as more specimens are exposed. Nevertheless, there was a clear transition between Stages 2 and 3, Fig. 9, so that values could be calculated for n_2 , k_2 , n_3 , and k_3 , Table IV. The experimentally-determined value of n_2 for this specimen was lower (0.40) than observed at 1300°C, while the observed transition point (x_{2-3}) was 28 μm , essentially the same as at 1300°C. In fact, the lifetimes calculated by the modified two-stage model using $n_2 = 0.4$ and the corresponding value of k_2 , and by using $n_2 = 0.5$ and the corresponding k_2 , were very similar (Table VI). Further, the lifetime of 4,455 h for the 1.04 mm-thick specimen predicted by the modified two-stage approach was close to the observed lifetime, 4,700 h, which was encouraging.

Data were available for two specimens exposed to 100h cycles at 1100°C for 10,000h or longer, as shown in Fig. 9, allowing the calculation of values for n_2 , k_2 , n_3 , k_3 , and x_{2-3} (Table IV). However, in this case $n_3 = 0.89$, suggesting that there may not yet be sufficient experimental data to obtain an overall value for k_3 . If the model is correct, these specimens may not be fully into Stage 3; spallation of oxide was observed from only the specimen edges after 10,000 h.

For a specimen exposed for 5,000 h (in 500h cycles) at 1000°C, a single, near-parabolic oxidation rate was followed throughout the exposure, Fig. 9, with no scale spallation observed. As a result, only values of n_2 and k_2 could be obtained experimentally. As shown in Table IV, the experimental value of n_2 was 0.37. A value of k_3 was obtained from an Arrhenius extrapolation using the higher-temperature k_3 values. Also, since there was an apparent trend for the values of x_{2-3} to decrease with temperature (Table IV), the higher-temperature values were used to extrapolate a value of x_{2-3} of 23 μm for 1000°C. At this point there is no indication that x_{2-3} should be independent of temperature, since factors contributing to loss of scale protectiveness probably change with temperature. For instance, relaxation of stresses developed in the scale may become easier with increasing temperature, so that an

argument could be made that n_{2-3} would increase with temperature. The use of these data in the modified two-stage calculation with the experimental value of $n_2=0.37$ and the corresponding value of k_2 resulted in lifetimes approximately double those obtained when a value of $n_2=0.5$ and the corresponding k_2 was used, Table VI. Again, there was obviously no way to verify these values from the experimental data available.

Figure 10 summarizes the predictions of lifetime as a function of temperature using eqn. 7 [with $(n_3 + f_{n3}) = 1.06$]. The current status of long exposure specimens at 1100°C is indicated. It is clear that it is vital to obtain more experimental data at 1100°-1200°C for MA956HT to verify the range of applicability of the modified multistage consumption methodology to this one alloy. Significantly more work is needed to examine its extension to other alloys.

Discussion

The initial choice in modeling is whether to use an existing model or to develop a new approach. Considering the models currently available, none appear to be inherently superior. The COSP model¹ is a two-stage model based on specimen mass change; the alloys for which it was developed exhibited an initial period of weight gain, followed by a period of uniform mass loss. The ASSET model² does not attempt to reproduce the mode of oxidation or the sequence of events in the oxidation process. Instead, it uses thermodynamic calculations to determine the overall mode of corrosion (oxidation, sulfidation, etc.), and then calculates the rate of metal loss from a database of experimental metal loss data, interpolating to the temperature, oxygen or sulfur partial pressure of interest through the use of appropriate algorithms. This approach provides data that are of immediate use to engineers, and appears to be appropriate for lower temperatures and alloys that exhibit internal oxidation and/or uniform metal loss. The Quadackers/Bennett approach³⁻⁵ was closest to the issues considered in the present study, and served as a basis for the application of the present multistage consumption model.

As mentioned above, the main reason for incorporating a multi-stage Al consumption model into life prediction was to reflect mass change in a manner that actually reflected what is measured (c.f. Fig.5). However, one of the underlying problems with this strategy is attaching physical significance to the third stage. This modified steady-state behavior is poorly understood and infrequently studied, judging by the sparsity of data in the oxidation literature. In order to develop confidence in the quantification of this stage, it would be useful to have a better understanding of how the metal-scale system transitions from Stage 2 to Stage 3, and more information on subsequent scale spallation and regrowth. For spallation, information is needed on the proportion of the alloy surface affected, the

relative influences of specimen corners and edges, the frequency of individual events, the type and amount of damage or defects necessary to cause spallation, and whether the damaged oxide remains attached to the specimen (i.e. non-protective scale¹⁰) or spalls. For the regrown oxide, little information is available on its microstructure. It has been suggested that such oxide is more porous and less protective than “virgin” grown scale⁵. The formation of a more defective scale could result in an inherently faster or temporarily-increased rate of growth, and lend physical significance to a Stage 2-Stage 3 transition scale thickness on the order of that observed here (20-30 μm). From a modeling standpoint, it also must be recognized that these types of effects likely will vary considerably among alloy systems.

In addition to the new inputs for a multi-stage model, the standard inputs for a single-stage model present some problems. In particular, values for $C_{B_i^*}$ (C_{B_b}) are difficult to obtain and can vary considerably depending on the type of alloy and oxidation temperature. For example, for very thin specimens, values for reactive element-alloyed FeCrAl appear to approach $C_{B_i^*} = 0$, with chromia layers observed forming below the alumina layer.¹¹ Recent work has even suggested that $C_{B_i^*}$ may be a function of specimen thickness for certain alloys.¹²

The experimental data for breakaway times is another area of concern. For the data in Figs. 2 and 3 there is surprising agreement for the ODS FeCrAl alloys with overall n values (lifetime vs. specimen thickness) of 0.63 to 0.85. However, recent work suggests that stronger ODS alloys may have lower n values than weaker cast FeCrAl alloys.¹² For another class of alloy, the Ni-based Haynes 214, the overall n value for was significantly different, 0.39, which may relate to the two-phase structure of the alloy. During oxidation involving 1h cycles at 1200°C, the alloy may have become depleted in the Al-rich phase, which could have resulted in rapid attack of the depleted zone, independent of specimen thickness. In that case, the lifetime would be relatively insensitive to specimen thickness, particularly for thicker specimens.

From the above discussion and other numerous examples, it is clear that the oxidation behavior of high-temperature alloys often does not conform to the simplifying assumptions normally used. While it is thought that in most cases the overall oxidation processes are similar, variables such as the physical dimensions of the specimen and the temperature dependence of the mechanical properties of the alloy substrate can significantly modify the duration of the different stages of oxidation, the morphology of the oxide formed, or the time to onset of oxide spallation. Any realistic model for high-temperature oxidation must be able to accommodate many of these features, so that it becomes important to develop mechanistic descriptions that are amenable to some form of quantification.

Summary

Based on experimental results for high-temperature FeCrAl alloys with excellent oxidation resistance, currently available models are not sufficient to describe the observed behavior. A method that attempts to link the mathematical description of the consumption rate of the scale-forming element with observed phenomena is needed. An approach is suggested that relies on breaking the steady-state consumption rate into multiple stages. In higher-temperature experiments these stages are clearly observed, whereas at more relevant, lower temperatures these stages are more difficult to observe within reasonable experimental times. Thus, it is necessary to develop criteria for the transition between the various stages of oxidation. Initial results showed reasonable predictions using this methodology for one alloy (MA956HT) at a very high temperature. However, in order to exactly match the observed lifetimes it was necessary to postulate a higher rate exponent or a higher oxidation rate than measured experimentally in the modified steady-state regime, or to postulate a significantly higher value for the minimum Al level for maintenance of the protective scale. These observations suggest that the oxidation mechanism in the modified steady state regime is more complicated than normally assumed. Clearly, extensive work will be required to determine the real potential for this approach, particularly for lower temperatures.

Acknowledgments

This research was sponsored by the Fossil Energy Advanced Research and Technology Development (ARM) Materials Program, U.S. Department of Energy, under contract DEA0596OR22725 with UT-Battelle, LLC. Thanks are due to Dr. G. Smith of INCO, Dr. D. Spörer of Metallwerk Plansee, and Mr. Q. J. Mabbutt of British Gas plc. for supplying samples of ODS-FeCrAl alloys. We would like to also acknowledge the contributions of colleagues at the Oak Ridge National Laboratory: L. D. Chitwood, G. W. Garner, and M. Howell for the oxidation testing, and M. P. Brady and D. F. Wilson for critically reviewing the manuscript.

References

1. C. E. Lowell, C. A. Barrett, R. W., Palmer, J. V. Auping and H. B. Probst, *Oxid. Met.*, 1991, 36, 81-112.
2. R. C. John, W. T. Thompson, and I. Karakaya, "Alloy corrosion data bases combined with thermochemical analysis," *CORROSION/88*, paper 136, NACE, Houston, Texas (1988).

3. W. J. Quadakkers and M. J. Bennett, *Mat. Sci. Technology*, 1994, 10, 126-131.
4. W. J. Quadakkers and K. Bongartz, *Werkst. Korros.*, 1994, 45, 232-41.
5. M. J. Bennett, H. Romary and J. B. Price, "The Oxidation Behavior of Alumina Forming Oxide Dispersion Strengthened Ferritic Alloys at 1200-1400°C," pp. 95-103 in *Heat Resistant Materials*, K. Natesan and D. J. Tillack, eds. (ASM, Materials Park, Ohio, 1991).
6. B. A. Pint, P. F. Tortorelli, and I. G. Wright, ORNL Laboratory Report (2001), in press.
7. B. Pieraggi, *Oxid. Met.*, 1987, 27, 177-85.
8. B. A. Pint, P. F. Tortorelli and I. G. Wright, "Effect of Cycle Frequency on High Temperature Oxidation Behavior of Alumina- and Chromia-Forming Alloys," p. 111-32 in M. Schütze and W. J. Quadakkers eds., *Cyclic Oxidation of High Temperature Materials*, The Institute of Materials, London, 1999.
9. See, for instance, I. G. Wright, V. K. Sethi, and A. J. Markworth, *Wear*, 1995, 186-187, 230-237.
10. F. H. Stott, F. A. Golightly and G. C. Wood, *Corr. Sci.*, 1979, 19, 889-906.
11. N. Hiramatsu and F. H. Stott, *Oxid. Met.*, 1999, 51, 479-94.
12. J. P. Wilber, M. J. Bennett and J. R. Nicholls, *Mater. High Temp.*, 2000, 17, 125-32.

List of Figures

- Fig. 1. Polished cross section of alloy MA956HT after 10,000 h (100 x 100-h cycles) at 1100°C. Optical microscopy. Only small amounts of spallation were observed and the cross sectional thickness was virtually unchanged within measuring accuracy.
- Fig. 2. Experimental data for the time to breakaway versus specimen thickness for specimens of alloys APM, MA956HT, and FAS+Hf exposed in 100-h cycles in air at 1300°C.
- Fig. 3. Experimental data for the time to breakaway versus specimen thickness for specimens of ORNL-made ODS-FeCrAl specimens exposed in 1-h cycles in air at 1200°C.
- Fig. 4. Experimental data for the time to breakaway versus specimen thickness for specimens of Haynes 214 exposed in 1-h cycles in air at 1200°C.
- Fig. 5. (a) Total mass gain data for specimens of alloy MA956HT exposed in 100-h cycles in air at 1300°C (b) Specimen mass gain data for specimens of alloy MA956HT exposed in 100-h cycles in air at 1300°C
- Fig. 6. Schematic diagram of oxidation kinetics of alloy MA956HT exposed in 100-h cycles in air at 1300°C
- Fig. 7. Comparison of observed and predicted oxidation lifetimes for alloy MA956HT exposed in 100-h cycles in air at 1300°C. (Initial 2-stage fit used: $n_2=0.5$; $n_3=1.0$ ($f_{n3}=0$); k_2, k_3 =average of data set; $\delta_{2-3}=29\mu\text{m}$; $C_{Bb}=1.2\%$. Modified 2-stage fits used same basis, with indicated changes in f_{n3} , or C_{Bb})
- Fig. 8. Sensitivity of two-stage model to changes in the values of the single variables (a) n_3 (b) k_3 (c) δ_{2-3} (d) C_{Bb} with all other parameters at the 'standard' values: $n_2=0.5$; $n_3=1.0$; k_2, k_3 =average for standard data sets for standard n values; $\delta_{2-3}=29\mu\text{m}$; $C_{Bb}=1.2\%$.
- Fig. 9. Experimental data for MA956HT oxidized at 1000°C in 500-h cycles, and at 1100 and 1200°C in 100-h cycles. (Basis: $< \delta_{2-3}$, oxidation is parabolic, $n_2=0.5$; $> \delta_{2-3}$, oxidation 'linear,' $n_3=1.0$; k_2, k_3 from averages of data set for $n_2=0.5, n_3=1.0$; $f_{n3}=0.06$; $C_{Bb}=1.2$)
- Fig. 10. Predicted lifetimes as a function of temperature. (Basis: $< \delta_{2-3}$, oxidation is parabolic, $n_2=0.5$; $> \delta_{2-3}$, oxidation 'linear,' $n_3=1.0$; k_2, k_3 from averages of data set for $n_2=0.5, n_3=1.0$; $f_{n3}=0.06$; $C_{Bb}=1.2$)

Table I. Chemical Compositions of Alloys Studied (weight percent)

Alloy	Fe	Ni	Cr	Al	Ti	Si	S*	O	Other
MA956HT	Bal.	0.11	21.6	5.9	0.4	0.05	50	0.21	0.38Y as Y ₂ O ₃
Kanthal APM	Bal.	—	20.4	5.5	0.03	0.23	10	0.05	0.10Zr as ZrO ₂
PM2000	Bal.	0.1	18.9	5.1	0.5	0.04	21	0.25	0.37Y as Y ₂ O ₃
FCA+Y ₂ O ₃	Bal.	0.1	19.7	4.9	<0.01	0.1	28	0.53	0.17Y as Y ₂ O ₃
FCA+La ₂ O ₃	Bal.	0.1	19.7	4.9	<0.01	0.1	31	0.36	0.06La as La ₂ O ₃
FAS+Hf	Bal.	<0.01	2.1	15.6	<0.01	<0.01	24	0.004	0.38Hf (0.10 at%)
Haynes 214	3.5	Bal.	15.6	4.3	0.01	0.1	3	0.001	0.02Zr, 0.004Y

*ppm wt

Table II. Summary of Factors that Complicate Modeling, Listed by Oxidation Stage

TRANSIENT OXIDATION	STEADY-STATE OXIDATION	MODIFIED STEADY-STATE OXIDATION	BREAKAWAY OXIDATION
SIMPLEST ASSUMPTIONS			
<ul style="list-style-type: none"> • short duration • sequence determined by T/D considerations 	<ul style="list-style-type: none"> • oxide thickens with time at a characteristic parabolic rate • T-dependence according to Arrhenius relationship • oxide is uniform in thickness • oxide is adherent 	<ul style="list-style-type: none"> • scale spallation initiates due to growth stresses • scale spalls to substrate-oxide interface • oxide regrowth follows same parabolic rate law • spallation initiates at a given oxide thickness 	<ul style="list-style-type: none"> • initiates when $C_{Bi} < C_{Bi}^*$ • $C_B = C_{Bi}$
COMPLICATING ISSUES			
<ul style="list-style-type: none"> • surface finish • substrate stress • spinel or M₂O₃-formation? • $C_B > C_{Bi}^*$ • desired crystal structure is critical 	<ul style="list-style-type: none"> • constant rate law dependence • pO₂ effects within range of stability of 'normal' oxide • water vapor effects 	<ul style="list-style-type: none"> • substrate thickness effects • edge effects—corners, sharp points • substrate strength • CTE mismatch, substrate vs oxide • substrate phase change • interface roughness • oxide thickness 	<ul style="list-style-type: none"> • rapid weight loss=onset of breakaway oxidation? • slope of concentration gradient of B • possibility of 'healing' inner layer of B₂O₃

Table III. Experimentally-Observed Lifetimes for MA956HT

Time to breakaway, h	Specimen Thickness, mm							
	0.97	1.04	1.24	1.51	1.78	1.94	1.98	2.23
1300°C	880	—	1,100	1,450	1,550	1,700	1,700	1,900
1200°C	—	4,700	—	—	—	—	—	—

Table IV. Summary of Experimental Data over the Temperature Range 1000-1300°C

Temperature °C	n_2	k_2 mgcm ⁻² h ^{-0.5}	$_{2-3}$ μm	n_3	k_3 mgcm ⁻² h ⁻¹
1300	0.52	0.236	29	1.03	12.49 x 10 ⁻³
1200	0.40	0.113	28	1.07	2.60 x 10 ⁻³
1100	0.52	0.066	25	0.89	0.70 x 10 ⁻³
1000	0.37	0.015	23*	—	0.13 x 10 ⁻³ *

*extrapolated

Table V. Sensitivity of Calculated Lifetime at 1300°C to Major Variables

n_3	k_3 (mgcm ⁻² h ⁻ⁿ³)	$_{2-3}$ (μm)	C_{Bb} (%)	t_b (%)*
1.00	0.012490	29	1.2	+39
1.03	0.009912	29	1.2	+40
1.05	0.008484	29	1.2	+41
1.07	0.007273	29	1.2	+42
1.10	0.005776	29	1.2	+42
Changes in individual variables to give best fit:				
1.00	k_3 x 1.5	29	1.2	+3
n_3 + 0.06	0.012490	29	1.2	+2
1.00	0.012490	29	2.5	+2
1.00	0.012490	0-40	1.2	No closure

* t_b calculated for the specimen thicknesses shown in Table II, and compared to the observed lifetimes.

Table VI. Oxidation Lifetimes Calculated Using a Multistage Approach

Temp °C	Model Inputs Used						2-Stage Model Predictions (h)		
	n_2	k_2^* mgcm ⁻² h ^{-0.5}	$_{2-3}$ μm	n_3	f_{n3}	k_3 mgcm ⁻² h ⁻¹	1.0 mm	1.5 mm	2.0 mm
1300	0.50	0.236	29	1.0	0	12.49 x 10 ⁻³	1,258	1,860	2,462
1300	0.50	0.236	29	1.0	0.06	12.49 x 10 ⁻³	1,005	1,388	1,761
1200	0.40	0.241	28	1.0	0.06	2.60 x 10 ⁻³	4,286	5,966	7,605
1200	0.50	0.113	28	1.0	0.06	2.60 x 10 ⁻³	4,312	5,992	7,631
1100	0.50	0.066	25	1.0	0.06	0.70 x 10 ⁻³	13,265	19,046	24,689
1000	0.37	0.046	23	1.0	0.06	0.13 x 10 ⁻³	218,635	245,988	272,703
1000	0.50	0.015	23	1.0	0.06	0.13 x 10 ⁻³	118,768	146,121	172,836

*corresponding to indicated n_2

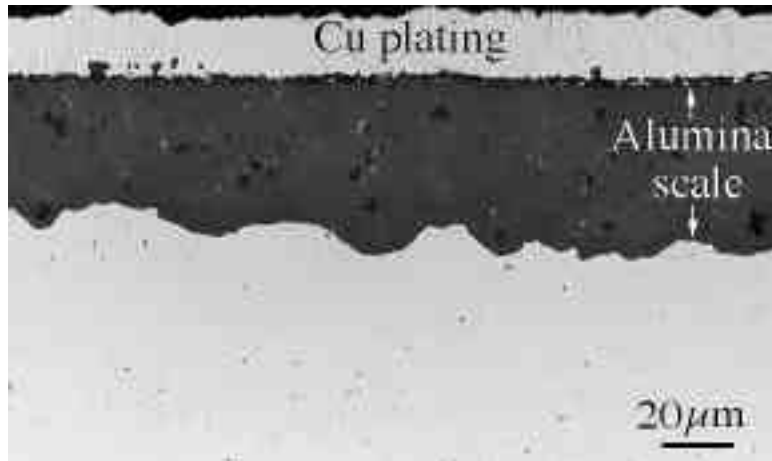


Fig. 1. Polished cross section of alloy MA956HT after 10,000 h (100 x 100-h cycles) at 1100°C. Optical microscopy. Only small amounts of spallation were observed and the cross sectional thickness was virtually unchanged within measuring accuracy.

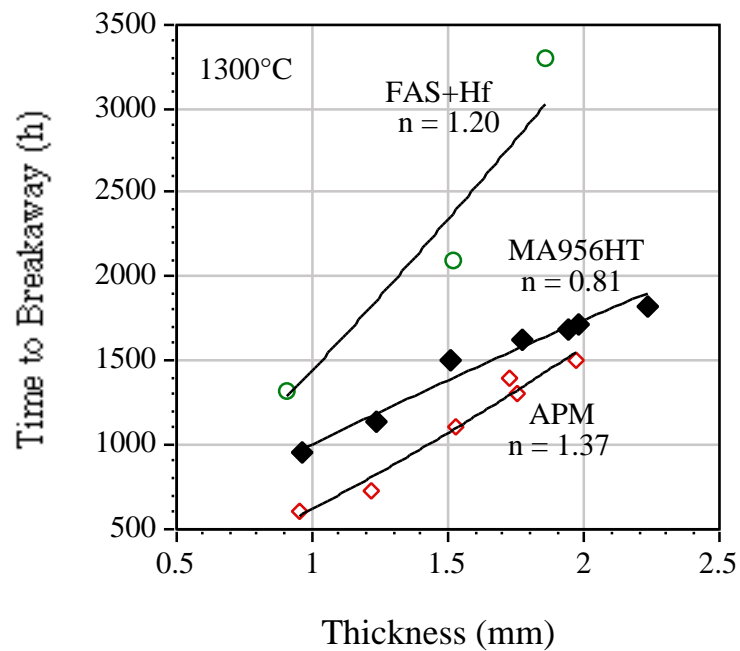


Fig. 2. Experimental data for the time to breakaway versus specimen thickness for specimens of alloys APM, MA956HT, and FAS+Hf exposed in 100-h cycles in air at 1300°C.

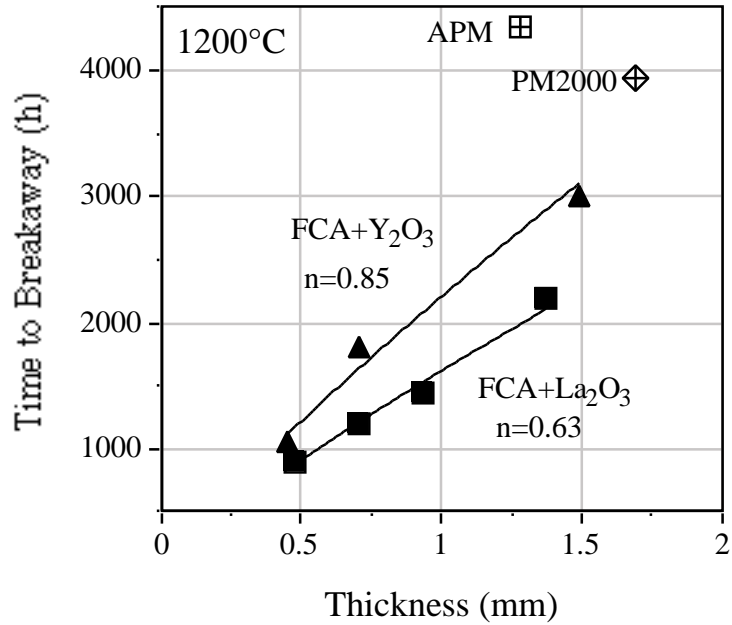


Fig. 3. Experimental data for the time to breakaway versus specimen thickness for specimens of ORNL-made ODS-FeCrAl specimens exposed in 1-h cycles in air at 1200°C.

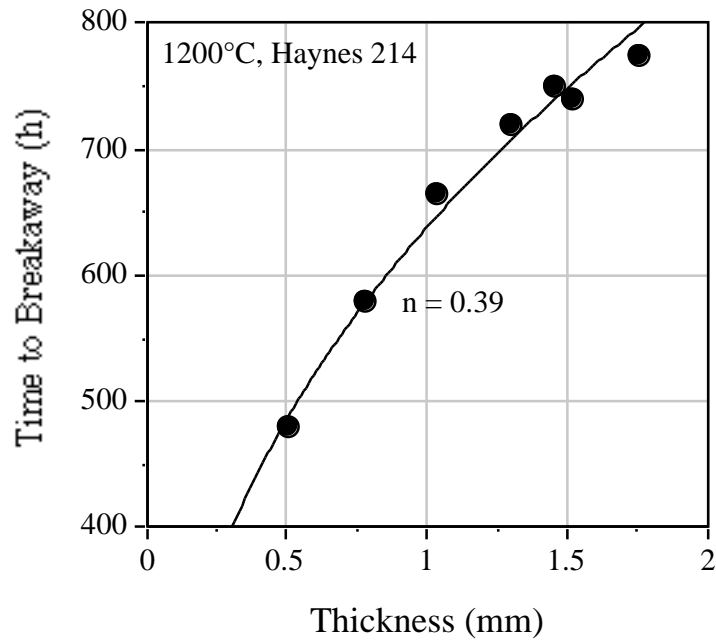


Fig. 4. Experimental data for the time to breakaway versus specimen thickness for specimens of Haynes 214 exposed in 1-h cycles in air at 1200°C.

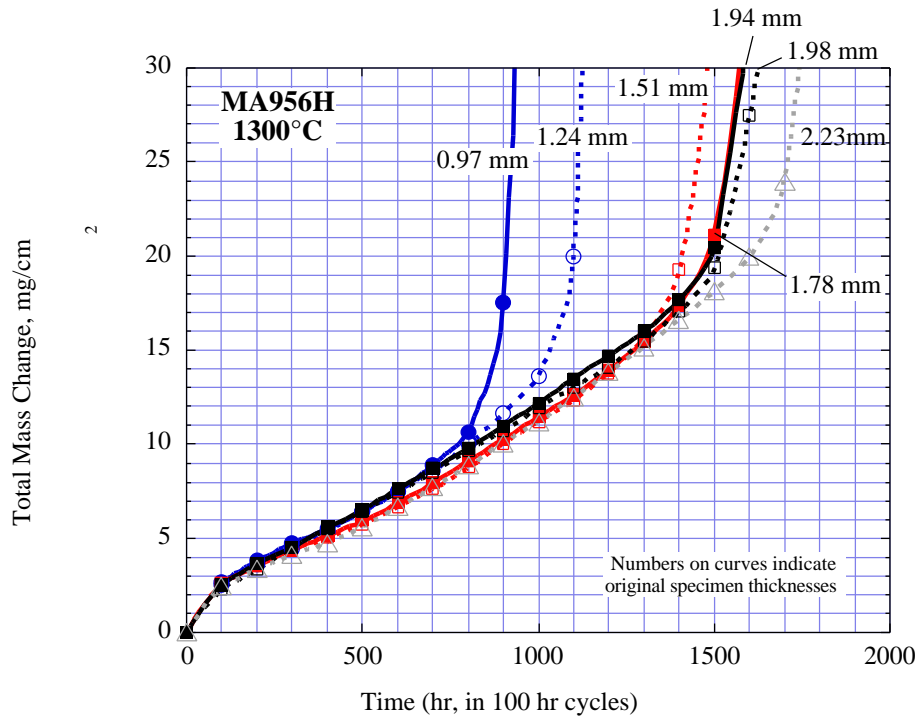


Fig. 5a. Total mass gain data for specimens of alloy MA956HT exposed in 100-h cycles in air at 1300°C

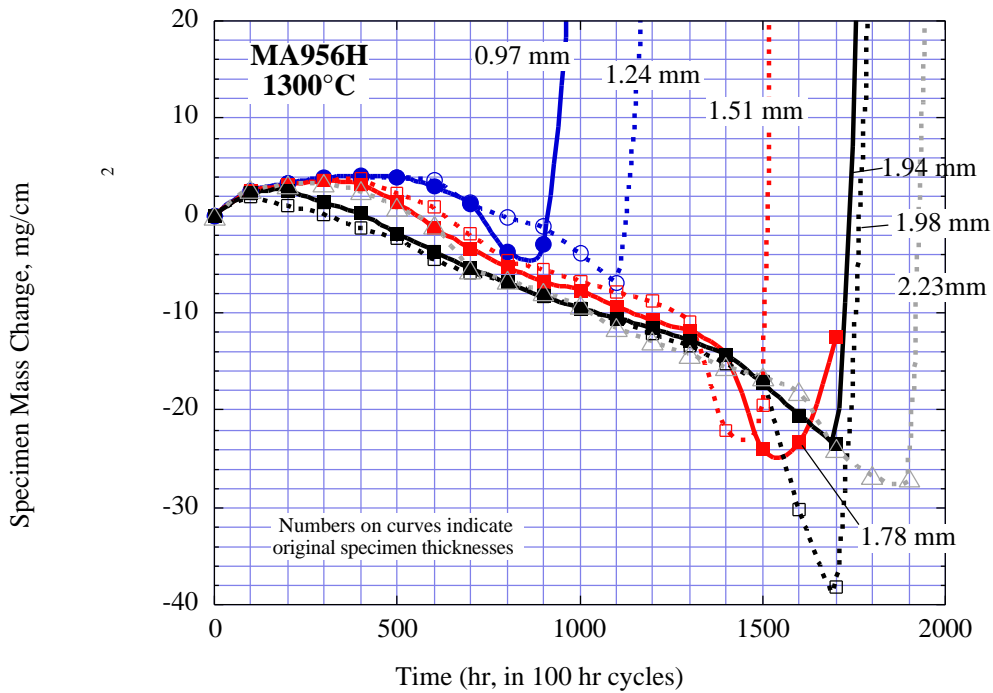


Fig. 5b. Specimen mass gain data for specimens of alloy MA956HT exposed in 100-h cycles in air at 1300°C

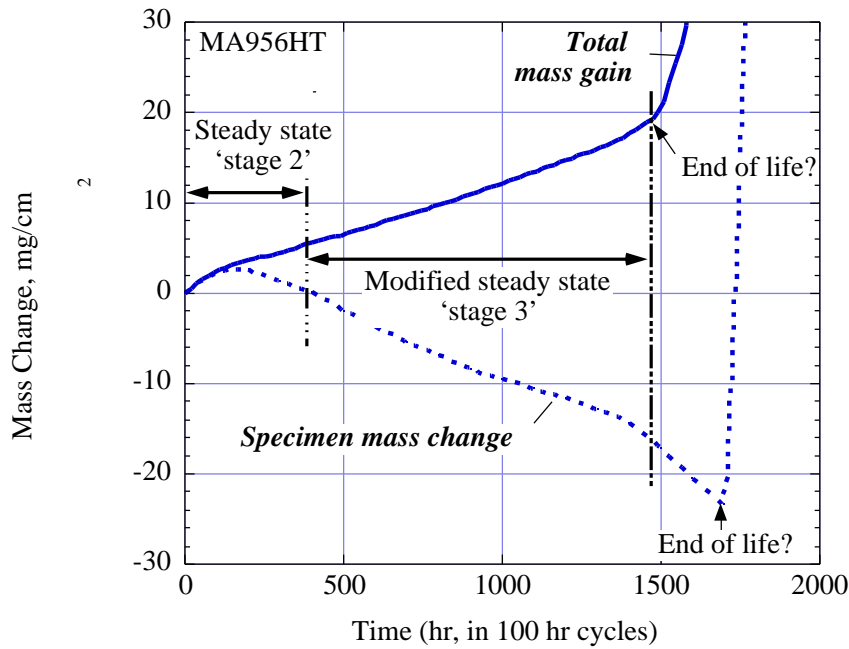


Fig. 6. Schematic diagram of oxidation kinetics of alloy MA956HT exposed in 100-h cycles in air at 1300°C

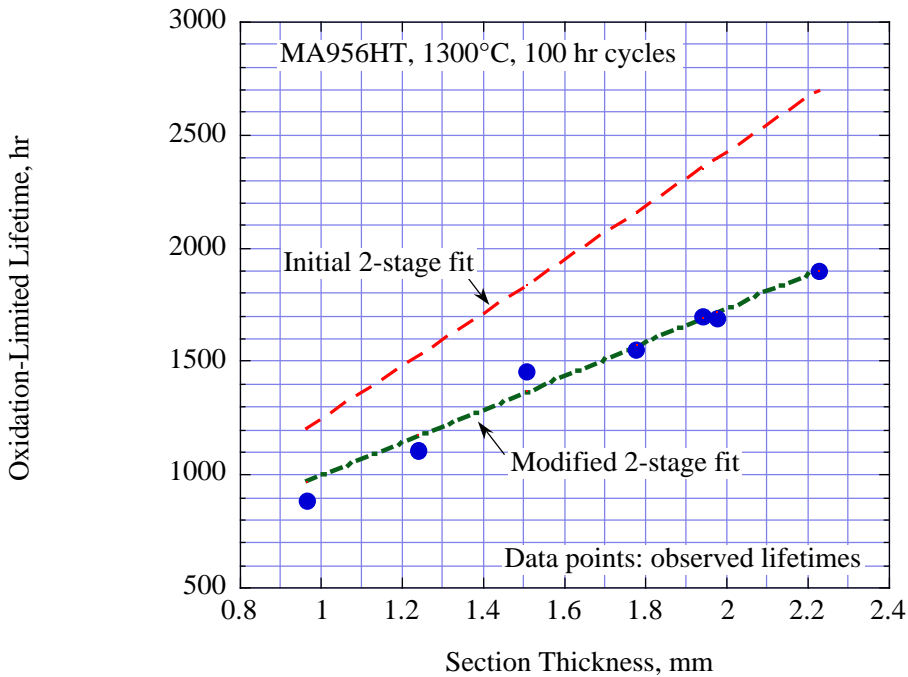
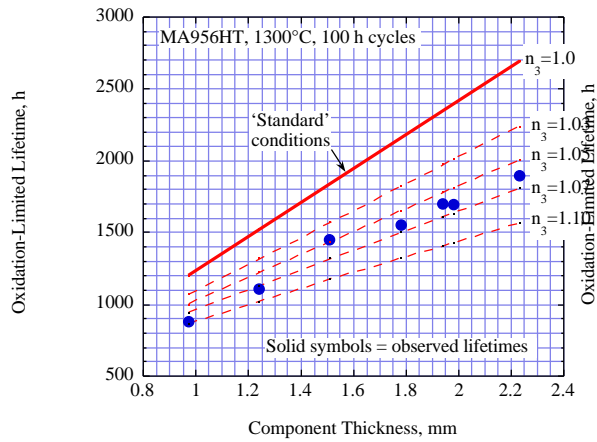
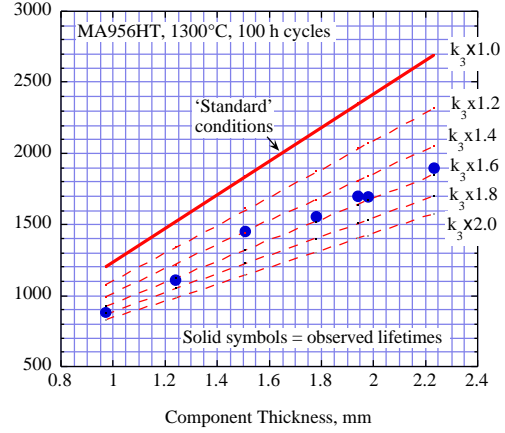


Fig. 7. Comparison of observed and predicted oxidation lifetimes for alloy MA956HT exposed in 100-h cycles in air at 1300°C.

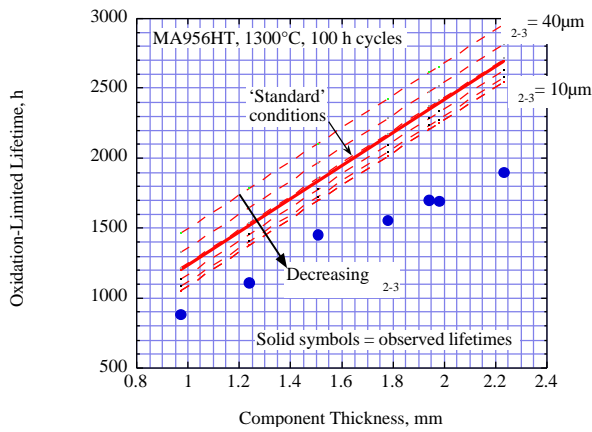
(Initial 2-stage fit used: $n_2=0.5$; $n_3=1.0$ ($f_{n_3}=0$); k_2, k_3 =average of data set; $\delta_{2-3}=29\mu\text{m}$; $C_{Bb}=1.2\%$.
 Modified 2-stage fits used same basis, with indicated changes in f_{n_3} , or C_{Bb})



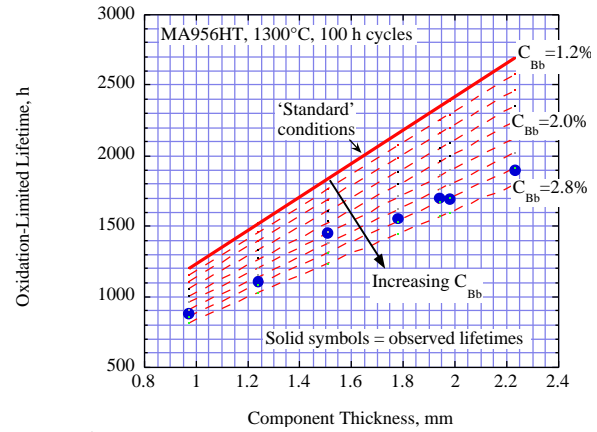
(a)



(b)



(c)



(d)

Fig. 8. Sensitivity of two-stage model to changes in the values of the single variables (a) n_3 (b) k_3 (c) $_{2-3}$ (d) C_{Bb} with all other parameters at the 'standard' values: $n_2=0.5$; $n_3=1.0$; k_2, k_3 =average for standard data sets for standard n values; $_{2-3}=29\mu\text{m}$; $C_{Bb}=1.2\%$.

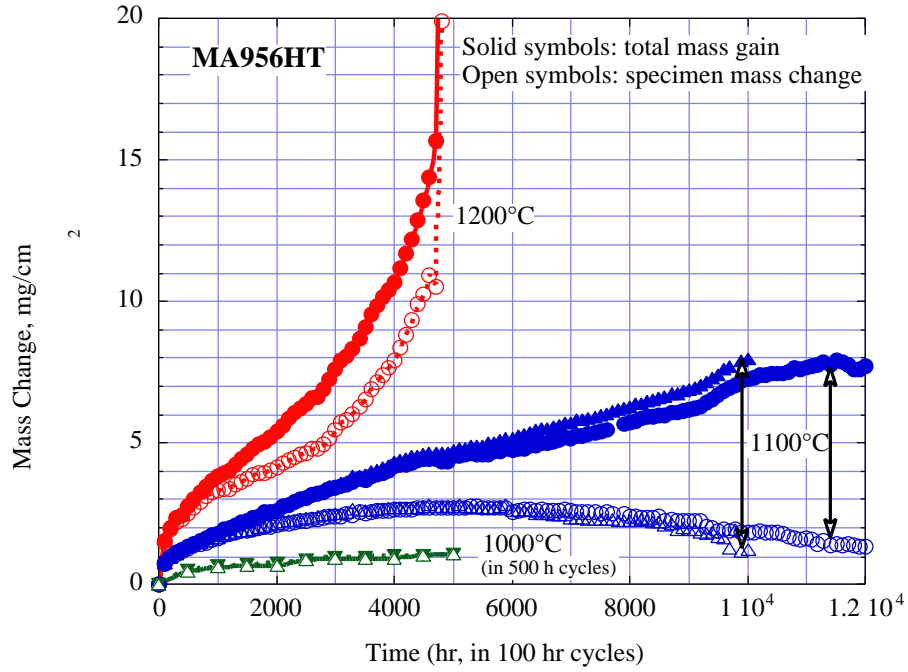


Figure 9. Experimental data for MA956HT oxidized at 1000°C in 500-h cycles, and at 1100 and 1200°C in 100-h cycles

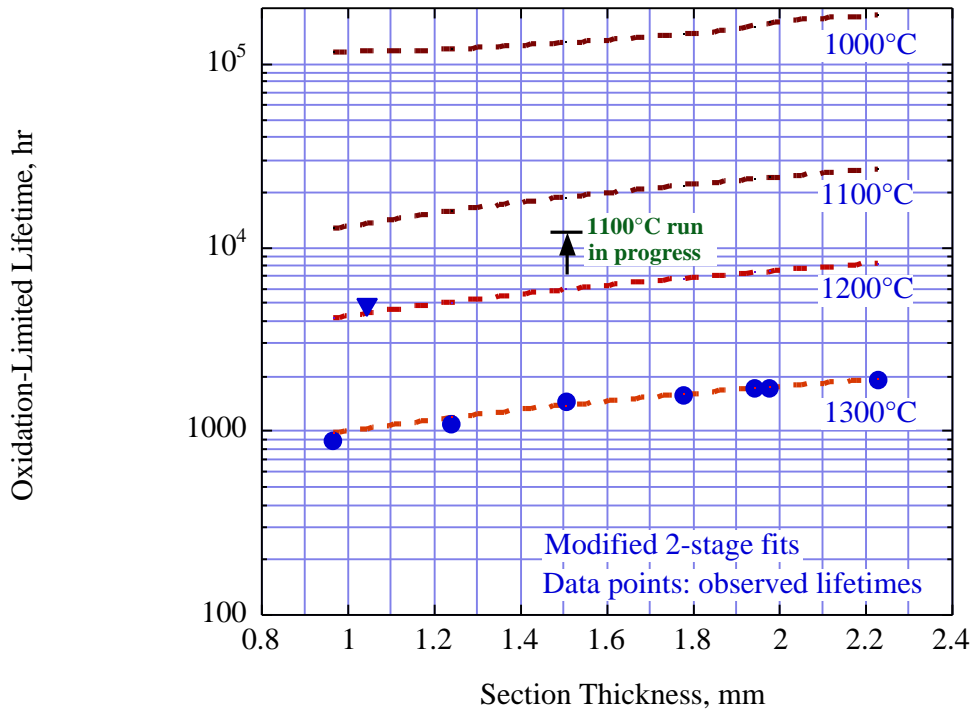


Figure 10. Predicted lifetimes as a function of temperature.
 (Basis: $<_{2-3}$, oxidation is parabolic, $n_2=0.5$; $>_{2-3}$, oxidation 'linear,' $n_3=1.0$; k_2, k_3 from averages of data set for $n_2=0.5, n_3=1.0$; $f_{n_3}=0.06$; $C_{Bb}=1.2$)